



ELSEVIER

Available online at [www.sciencedirect.com](http://www.sciencedirect.com)

SCIENCE @ DIRECT®

Journal of Applied Geophysics 54 (2003) 191–202

JOURNAL OF  
APPLIED  
GEOPHYSICS

[www.elsevier.com/locate/jappgeo](http://www.elsevier.com/locate/jappgeo)

# The effect of fluid saturation in an anisotropic multi-scale equant porosity model

Mark Chapman\*, Sonja Maultzsch, Enru Liu, Xiang-Yang Li

*Edinburgh Anisotropy Project, British Geological Survey, Murchison House, West Mains Road, Edinburgh, EH9 3LA, UK*

## Abstract

It is recognised that exchange of fluid between fractures and the rock matrix can have a strong impact on a rock's anisotropic elastic properties. A recent theoretical advance considers the effect of the scale length of the fractures. We show that under certain circumstances, this model can be simplified. The simplified model matches laboratory data. A prediction of the model is that frequency-dependent effects are important for fluid substitution in the anisotropic case.

© 2003 Elsevier B.V. All rights reserved.

*Keywords:* Anisotropic; Saturation; Equant

## 1. Introduction

It was demonstrated by [Thomsen \(1995\)](#) that the exchange of fluid between fractures and equant porosity during the passage of a seismic wave could have a profound effect on the calculated anisotropic elastic properties. The possibility of flow into equant porosity increases the compliance of the fracture set. A consequence of this is that theories, which neglect fluid flow may predict an incorrect dependence on the fluid bulk modulus.

[Thomsen's \(1995\)](#) model was based on the low frequency limit. [Hudson et al. \(1996\)](#) and [Tod \(2001\)](#) attempted to extend Thomsen's ideas to the entire frequency range. Various flow mechanisms were considered, including flow on a wavelength scale, flow

between cracks of different orientations and flow between the fractures and the rock matrix. A further model has been presented by [van der Kolk et al. \(2001\)](#).

[Chapman \(2003\)](#) gave a model which focused on the effect of the scale length of the fractures. In the absence of the fractures, the model returns to the grain-scale squirt flow model constructed by [Chapman \(2001\)](#). With the introduction of a fracture set, we find that there emerges two characteristics; the traditional squirt flow frequency, which has been estimated from laboratory data ([Murphy, 1985](#)), together with a lower characteristic frequency which depends on the size of the fractures. A consequence of this is that propagation at seismic frequencies can be very different from that predicted in the low-frequency limit.

In this paper, we examine further the predictions of the [Chapman \(2003\)](#) model. We propose a method for applying the model in the case where high porosity prevents the identification of the reference elastic moduli with any physically relevant parameters. With this technique, the model can often be simplified,

\* Corresponding author. Tel.: +44-131-667-1000; fax: +44-131-667-1877.

E-mail address: [m.chapman@bgs.ac.uk](mailto:m.chapman@bgs.ac.uk) (M. Chapman).

increasing greatly the practical applicability of the theory. We test our approximations by applying the simplified model to the laboratory measurements of Rathore et al. (1995). The results are satisfactory. Finally, we examine the effect of saturation on the predicted anisotropy. Fluid viscosity is found to play an important role.

## 2. Parameterisation

The model presented by Chapman (2003), the main results of which are summarised in Appendix A, assumed that pore space consisted of an isotropic distribution of grain-scale cracks and pores and a set of aligned fractures. The fractures were allowed to be larger than the grain-scale, but still had to be smaller than a seismic wavelength.

An advantage of the model was that it offered an explicit description of the “equant” in the rock. For a rock without fractures, the model is consistent with Gassmann’s formulae, allowing account to be taken of saturation changes. The derivation of the model followed Eshelby’s (1957) “Interaction Energy” approach to finding the elastic constants, and as such, was formally restricted to low porosities. Techniques such as the self-consistent method and the differential scheme (Christensen, 1980; Zimmerman, 1991) have been proposed to extend the analysis to higher porosities. While these techniques are not mathematically rigorous, it is hoped that they may be more accurate for higher porosities.

Hudson et al. (2001) showed that Rathore et al.’s (1995) velocity measurements on synthetic sandstone with controlled fracture geometry could be relatively successfully modelled with an equant porosity model which did not contain an explicit mechanical description of the porosity. The reference elastic moduli  $\lambda$  and  $\mu$  were taken from the measurements of velocity in the unfractured medium. This highlights a twin advantage of the traditional Hudson (1980, 1981) theory. The reference, or background, elastic moduli, which appear in the Hudson theory can easily be identified with physically meaningful quantities in the unfractured rock velocities. Moreover, it appears that these same parameters happen to be the correct quantities from which to calculate the fracture-induced corrections to the velocities.

As it stands, the model of Chapman (2003) does not share these advantages. The reference moduli  $\lambda$  and  $\mu$  should be derived from the velocities of rock without any cracks or pores, in other words, the grain moduli. However, the restriction to low porosity means that in practice,  $\lambda$  and  $\mu$  will themselves have to be fitted to achieve agreement with the background velocities. We expect that the use of these moduli to calculate the effect of fractures could result in substantial errors. Additionally, it is inconvenient for the user of the model to have to specify parameters, which do not have a convenient physical interpretation.

We now propose a method, similar in spirit to the self-consistent scheme, which circumvents these difficulties. Our assumption is that we know the velocities in the unfractured rock,  $V_p^o$  and  $V_s^o$ , at some frequency  $\omega_0$ . From these velocities, we derive moduli  $\lambda^o$ ,  $\mu^o$  as:

$$\mu^o = (V_s^o)^2 \rho; \quad (1)$$

$$\lambda^o = (V_p^o)^2 \rho - 2\mu^o; \quad (2)$$

where  $\rho$  is the density of the saturated rock.

For isotropic unfractured rock, the model of Chapman (2003) takes the form:

$$\lambda_{\text{eff}} = \lambda - \Phi_{c,p}[\lambda, \mu, \omega_0]; \quad (3)$$

$$\mu_{\text{eff}} = \mu - \Phi_{c,p}[\lambda, \mu, \omega_0]; \quad (4)$$

where the functions  $\Phi_{c,p}$  are perturbations due to the presence of micro-cracks and pores. Precise expressions for  $\Phi_{c,p}$  in terms of the porosity  $\Phi_p$  and crack density  $\epsilon_c$  follow from the formulae quoted in Appendix A. We wish to ensure that at frequency  $\omega_0$  and in the absence of fractures:

$$\lambda_{\text{eff}} = \lambda^o; \quad (5)$$

$$\mu_{\text{eff}} = \mu^o. \quad (6)$$

We do not, however, wish to choose non-physical  $\lambda$  and  $\mu$  to ensure that this is so since the corrections to the velocities, which what we are most interested in, would then be non-physical. Instead, we insist that the

corrections are calculated with the physical values  $\lambda^o$  and  $\mu^o$ . In other words, we must have:

$$\lambda^o = A - \Phi_{c,p}[\lambda^o, \mu^o, \omega_0]; \quad (7)$$

$$\mu^o = \mathcal{T} - \Phi_{c,p}[\lambda^o, \mu^o, \omega_0]. \quad (8)$$

It should be noted that  $A$  and  $\mathcal{T}$  are frequency independent, and represent reference constants. Although they have no direct physical meaning, they can be calculated from the measurable values  $V_p^o$  and  $V_s^o$ . We now propose to calculate our frequency dependent, anisotropic, elastic tensor as:

$$\begin{aligned} C_{ijkl}(\omega) = & C_{ijkl}^{\text{iso}}(A, \mathcal{T}) - \epsilon_c C_{ijkl}^1(\lambda^o, \mu^o, \omega) \\ & - \phi_p C_{ijkl}^2(\lambda^o, \mu^o, \omega) \\ & - \epsilon_f C_{ijkl}^3(\lambda^o, \mu^o, \omega); \end{aligned} \quad (9)$$

where  $C^{\text{iso}}(A, \mathcal{T})$  is the isotropic elastic tensor with Lamé parameters  $A$  and  $\mathcal{T}$  and  $\epsilon_f$  is the density of the aligned fractures.  $C^1$ ,  $C^2$  and  $C^3$  are functions of the Lamé parameters, fluid properties, fracture length, time scale parameter  $\tau$  and frequency. precise forms of these relationships are given in Appendix A.

The model of Chapman (2003) is fully consistent with the Brown and Korrिंगa (1975) at zero frequency. However, when we make the above modification, the theory is no longer strictly true; the elastic tensor is the sum of a Brown and Korrिंगa (1975) anisotropic tensor and an isotropic “correction” tensor. It is easy to overstate importance of consistency with Brown and Korrिंगa (1975). The formula gives a relationship the dry and saturated anisotropic elastic tensors. If, as is usually the case when rocks of high porosity, the dry elastic tensor is wrongly predicted then, the tensor predictions will also be in error, even when the relationship is satisfied. We believe our approach is an acceptable compromise between the need to account for high porosity and the need to be consistent with Brown and Korrिंगa (1975).

### 3. The effect of micro-crack density

In the attempt to predict velocity from the mineral moduli and inclusion geometry, the micro-crack den-

sity  $\epsilon_c$  plays a vital role. Despite their lack of porosity, thin cracks can have a strong impact on the elastic properties of a rock. The opening and closing of micro-cracks has long been recognised (Nur, 1971) as the dominant effect controlling the response of the elastic properties of rock to changes in effective stress. In our model, moreover,  $\epsilon_c$  plays a controlling role, with porosity, in determining the magnitude of dispersion at the squirt flow frequency.

Our model will often be applied, however, at seismic frequencies which are believed to usually be below the squirt flow frequency (Mavko et al., 1998). Requiring the unfractured velocities as inputs circumvent the problem of attempting to predict velocity from the mineral moduli and microstructure. Prediction of the effect of stress changes will only be required in time-lapse studies.

There is, therefore, a class of problems for which  $\epsilon_c$  appears to be irrelevant. It is hard to estimate  $\epsilon_c$  in practice, and requiring to do this complicates considerably the use of the model. For these reasons, we wish to investigate the feasibility of removing  $\epsilon_c$  from the model.

We assume first a brine-saturated rock, the brine properties following from Table 1, with unfractured velocities  $V_p = 4000 \text{ ms}^{-1}$  and  $V_s = 2500 \text{ ms}^{-1}$  at 100 Hz. The grain size is 200  $\mu\text{m}$ , and we consider the case of zero porosity. We take the time scale parameter  $\tau_m$  to be  $2 \times 10^{-5} \text{ s}$  to simulate the case where squirt flow frequency lies between the sonic and ultrasonic bands (Thomsen, 1995). (Note that the identification of  $1/\tau_m$  with the accepted notion of “squirt flow frequency” has been discussed by Chapman et al. (2002).) We now introduce a set of aligned fractures with density 0.05 and radius 1 m.

In Fig. 1, we plot percentage shear wave splitting (defined to be  $100 \times (S1 - S2)/S1$ , where  $S1$  is the pure-shear velocity and  $S2$  is the quasi-shear velocity) at an angle of  $70^\circ$  to the fracture normal for a range of frequencies. We consider the cases where  $\epsilon_c$  is set at 0.02, 0.04, 0.06 and 0.08. It can be seen that the

Table 1  
The fluid properties used in the calculations

	Brine	Oil	Gas
Acoustic velocity ( $\text{ms}^{-1}$ )	1710	1250	620
Density ( $\text{kg m}^{-3}$ )	1100	800	65
Viscosity (Pa s)	$1 \times 10^{-3}$	$2 \times 10^{-2}$	$2 \times 10^{-5}$

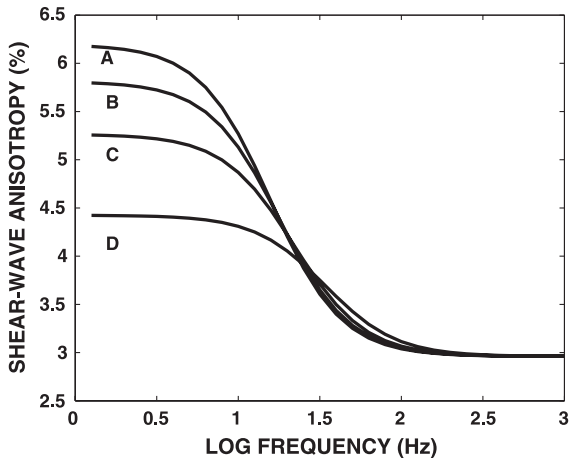


Fig. 1. Shear-wave anisotropy for propagation at 70 degrees to the fracture normal for  $\epsilon_c$  of (A) 0.08, (B) 0.06, (C) 0.04, (D) 0.02. Equant porosity is 0%.

model exhibits substantial sensitivity to  $\epsilon_c$ . Similar sensitivity can be observed in the variations of velocity with frequency and angle over the seismic frequency band. Clearly in this case, it is important not to attempt to simplify the model by setting  $\epsilon_c$  equal to zero arbitrarily.

In Fig. 2, we repeat the analysis, with the porosity changed to 10%. The sensitivity seen in the previous example largely disappears. In this case, it appears

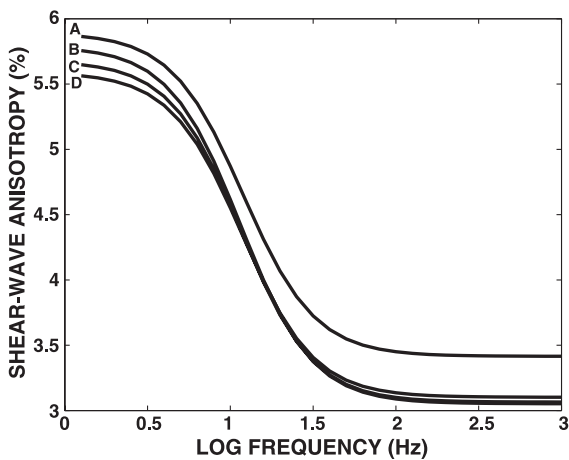


Fig. 2. Shear-wave anisotropy for propagation at 70 degrees to the fracture normal for  $\epsilon_c$  of (A) 0.08, (B) 0.06, (C) 0.04, (D) 0.02. Equant porosity is 10%.

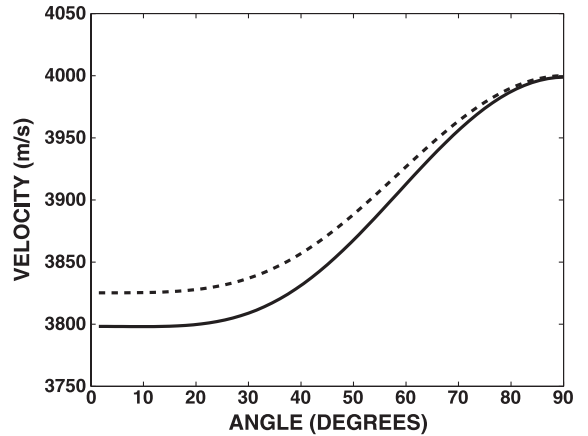


Fig. 3. qP velocity as a function of angle for 10% equant porosity,  $V_p^o = 4000 \text{ ms}^{-1}$ ,  $V_s^o = 2500 \text{ ms}^{-1}$ , and frequency 40 Hz. The dashed line assumes  $\epsilon_c = 0.05$ , the solid line assumes  $\epsilon_c = 0$ .

that there is a possibility of being able to simplify the model.

We now assume that in fact  $\epsilon_c = 0.05$  and investigate the error which would accrue from assuming  $\epsilon_c = 0$ . In Fig. 3, we reproduce the angular variation of the qP velocity at a frequency of 40 Hz assuming  $\epsilon_c = 0.05$  (dashed line) and  $\epsilon_c = 0$  (solid line). It can be seen that there is only a small difference between the two cases, with the maximum error occurring at angles close to  $0^\circ$ . Fig. 4 shows the results for shear wave propagation. The velocity of the pure-shear wave is

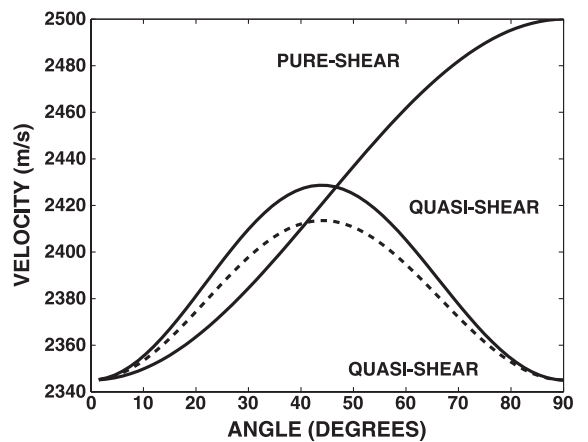


Fig. 4. Shear velocity as a function of angle for 10% equant porosity,  $V_p^o = 4000 \text{ ms}^{-1}$ ,  $V_s^o = 2500 \text{ ms}^{-1}$ , and frequency 40 Hz. The dashed lines assume  $\epsilon_c = 0.05$ , the solid lines assume  $\epsilon_c = 0$ .

independent of our assumption of  $\epsilon_c$ , and the quasi-shear wave shows only small dependence.

The reason for the difference between the 0% and 10% cases is physically clear. For the equant porosity effect to operate, fluid has to be able to flow out of the fracture into the background rock. This requires that there is sufficient porosity to accommodate the expelled fluid. When porosity is high, this condition is met satisfactorily. For the case of zero porosity, however, the expelled fluid is forced into the micro-cracks. The extent to which this is possible depends on the density of the micro-cracks, and this leads to the dependence of the behaviour on  $\epsilon_c$ .

We expect that, in most cases, the background porosity should be larger than the porosity associated with the fractures, and therefore, the assumption that  $\epsilon_c = 0$  should be reasonable. Nevertheless, it should be borne in mind that this simplification is only valid if there is sufficient porosity. For rocks of very low porosity, the dependence of the behaviour of the fractures on  $\epsilon_c$  gives rise to a novel time-lapse effect. Even under the assumption that the fractures themselves do not respond to pressure changes, changes in the micro-crack density can cause the behaviour of the fractures to change.

#### 4. Application of the model to laboratory data

We used the above interpretation of Chapman's (2003) theory to model the data presented by Rathore et al. (1995). The phase velocity measurements were performed on synthetic sandstone samples with known fracture geometry and porosity. Data for an unfractured but porous dummy sample were also provided. Thus, most parameters required by the model are. In fact, the approach described above allows us to reduce the fitting to one free parameter, which is the relaxation time  $\tau_m$ .

Fig. 5 shows the results of the modelling for fluid-filled fractures. We have chosen a matrix with only circular pores and no micro-cracks. Since the equant porosity in the synthetic samples is very high (35%), it makes hardly any difference in the modelling if part of the spherical pores is replaced with micro-cracks.

Overall, the modelled velocities shown in Fig. 5 match the measured data reasonably well. The time scale parameter  $\tau_m$ , which has a value of  $7.7 \times 10^{-7}$  s

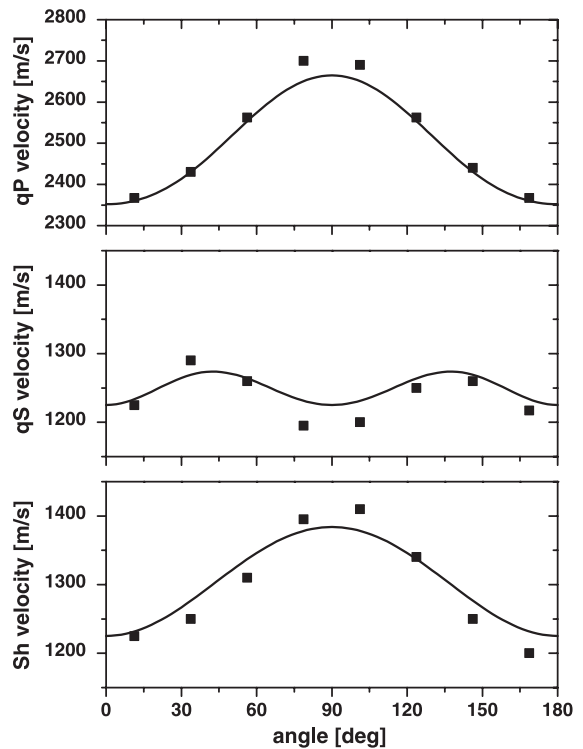


Fig. 5. Comparison of the Rathore et al. (1995) data set for saturated synthetic sandstone with our modelling. The curves were fit by setting  $\tau_m = 7.7 \times 10^{-7}$  s.

in the presented results, has a strong influence on the degree of polar variation of qP and qS velocities in the saturated case. The deduced value fits the data slightly better than the  $\tau_m = 0$  limit, which must be emphasised, gives a good fit to the data itself.

Hudson et al. (2001) discussed in great detail the differences between the equant porosity models given by Thomsen (1995) and Hudson et al. (1996), as well as the results of fitting the theories to the above data for fluid-saturated fractures. It was found that first-order expressions gave a better match than second-order ones. Hudson et al. (2001) also pointed out that the wavelengths used in the measurements are not long enough compared to the size of the fractures for effective medium theories to be strictly applicable. Therefore, a detailed quantitative comparison of data and modelling cannot be made. Nevertheless, the experiments provide a good tool to check predictions of effective medium theories in a more qualitative

way. With that in mind, the results shown here support our proposed methodology.

## 5. The effect of saturation

We now proceed to consider the effect of saturation on the anisotropy. Three different saturating fluids will be considered; brine, oil and gas. The physical properties, which we assume for these fluids, are given in Table 1.

In general, there are three physical effects which the model takes into account in the fluid substitution problem. The first is the density effect. When one fluid is replaced by another, the density of the saturated rock changes and this results in variations in all the velocities. There is also a fluid bulk modulus effect, in that the incompressibility the fluid contributes to the incompressibility of the composite. This is the traditional Gassmann (1951), or in the anisotropic case, Brown and Korringa (1975) effect. However, the fluid viscosity also makes a contribution to the fluid substitution problem. The time scale constant  $\tau_m$  is proportional to fluid viscosity, implying that the effect of changing viscosity is similar to the effect of changing frequency. Understanding frequency dependence is therefore important to perform fluid substitution correctly.

In the calculations we have performed so far, we have begun with “unfractured rock” velocities  $V_p^o$  and  $V_s^o$ . These typically depend on saturation. Our model, however, takes account of saturation through variation in the fluid density, bulk modulus and viscosity, not through variation in  $V_p^o$  and  $V_s^o$ . We therefore demand that the same  $\lambda^o$ ,  $\mu^o$ ,  $A$  and  $\mathcal{T}$  are used for each saturation. If we failed to impose this condition, we would, in effect, be including the same compressibility effect twice, once to change  $V_p^o$  and  $V_s^o$  and then again in the correction proportional to  $\Phi_p$ .

We assume, once again,  $V_p^o = 4000 \text{ ms}^{-1}$  and  $V_s^o = 2500 \text{ ms}^{-1}$ , a 10% porosity and for brine saturation,  $\tau_m = 2 \times 10^{-5} \text{ s}$ . Since  $\tau_m$  is directly proportional to fluid viscosity, we have from Table 1 that the  $\tau_m$  for oil saturations is  $4 \times 10^{-4} \text{ s}$  and for gas saturation  $\tau_m$  must be  $4 \times 10^{-7} \text{ s}$ .  $V_p^o$  and  $V_s^o$  are converted to  $\lambda^o$  and  $\mu^o$  with the properties of the brine-saturated rock. We introduce a fracture set with fracture density 0.05 and fracture radius 1 m. The fracture density controls only the strength of the

anisotropy; the qualitative behaviour of the model is insensitive to this parameter. Crack density is set to zero following the discussion in Section 3.

Fig. 6 shows the predicted variation of qP-velocity with frequency for propagation at an angle of  $45^\circ$  to the fracture normal for the three saturations. The gas-saturated velocity is substantially lower than the oil- and brine-saturated velocities at low frequencies. This is due to the Gassmann effect in the pores; the gas has a lower bulk modulus than the oil and brine, and this dominates the smaller density of the gas. In the zero frequency limit, the brine-saturated velocity is higher than the oil-saturated, but at higher frequencies, the effect of the higher oil viscosity becomes important and the oil-saturated velocity overtakes the brine-saturated velocity.

In Fig. 7, we repeat the analysis for the quasi-shear wave. For an isotropic rock, Gassmann’s formulae predict that the shear modulus is unaffected by saturation. This is no longer true in the anisotropic case; Brown and Korringa (1975) showed that fluid compressibility can affect shear wave propagation in this case. For this reason, brine-saturated and oil-saturated velocities are higher than the gas-saturated velocity at low frequency. The high viscosity of the oil leads to that velocity being the highest for frequencies around 1 Hz. At higher frequencies, the fluid compressibility contrast becomes less important (Chapman, 2001). For this reason at a frequency of 1 kHz, the lower density of the gas begins to dominate the higher bulk

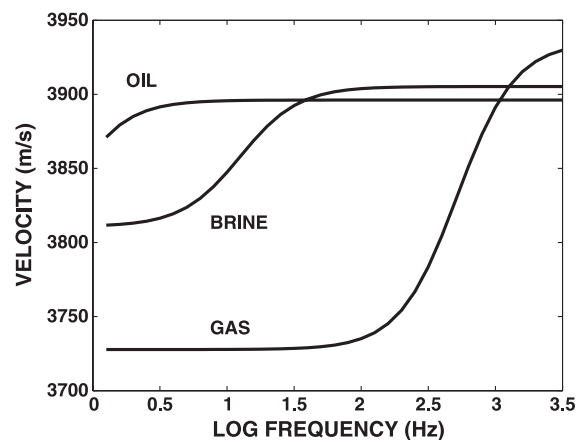


Fig. 6. qP velocity for propagation at  $45^\circ$  to the fracture normal as a function of frequency for three different saturations. Fracture size is 1 m.

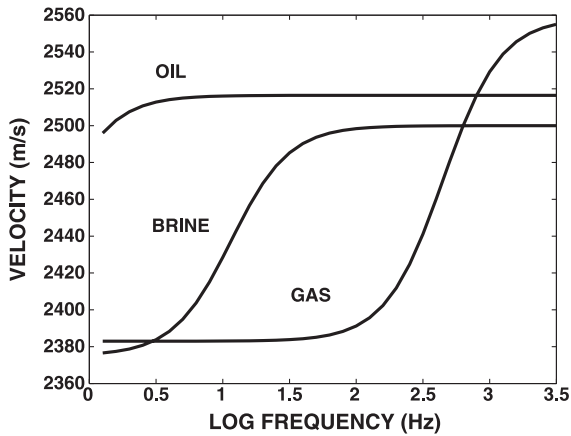


Fig. 7. Quasi-shear velocity for propagation at 45° to the fracture normal as a function of frequency for three different saturations. Fracture size is 1 m.

moduli of the oil and brine and the gas-saturation has the highest velocity.

Fig. 8 shows the analysis for the pure shear wave. A pure shear wave does not compress the fractures, so fluid flow between the fractures and the rest of the rock is not an important mechanism. The differences in the velocities reflect the different densities of the pore fluids, with the exception of the increase in oil velocity below 1 kHz. This is the standard squirt flow effect between micro-cracks and pores. It is independent of the fractures, and occurs for oil saturation at low frequency because of the high viscosity of the oil.

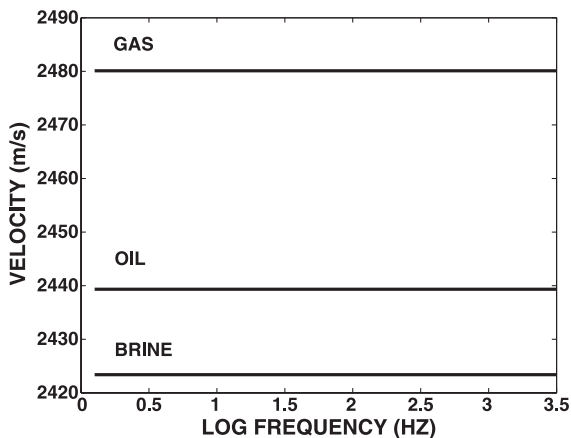


Fig. 8. Pure-shear velocity for propagation at 45° to the fracture normal as a function of frequency for three different saturations. Fracture size is 1 m.

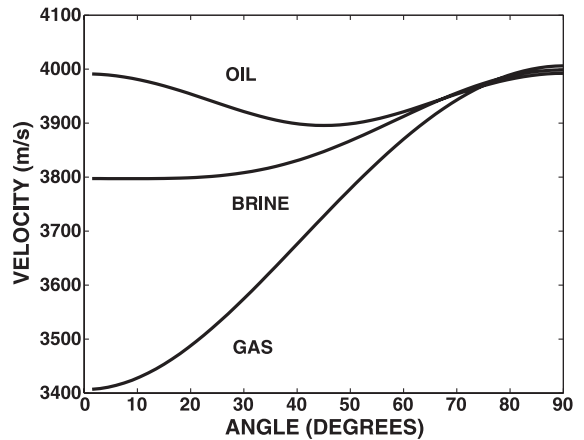


Fig. 9. qP velocity as a function of angle for three saturations. The frequency is 10 Hz and the fracture size is 1 m.

In Fig. 9, we show qP velocity as a function of angle for the three saturations, at frequency of 10 Hz. As expected, the gas saturation has the lowest velocity due to the Gassmann effect. For propagation at 90° which is less affected by the fractures, brine saturation has a higher velocity than oil saturation due once again to the Gassmann effect. At lower angles, however, the fractures begin to play a role and therefore fluid viscosity becomes important. For angles of 0°, the oil-saturated velocity is higher than the brine-saturated velocity.

Fig. 10 shows identical analysis for the case of the quasi-shear wave. When propagation is at 90°

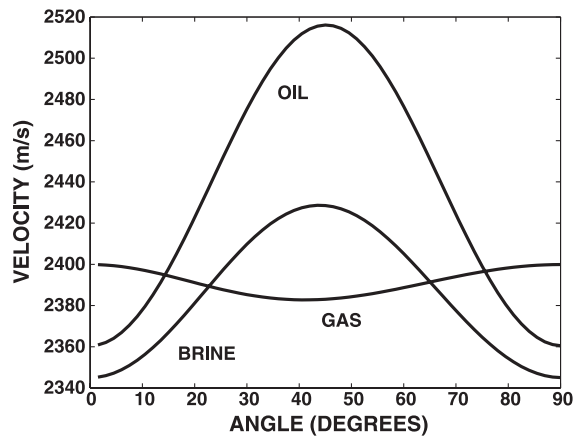


Fig. 10. Quasi-shear velocity as a function of angle for three saturations. The frequency is 10 Hz and the fracture size is 1 m.

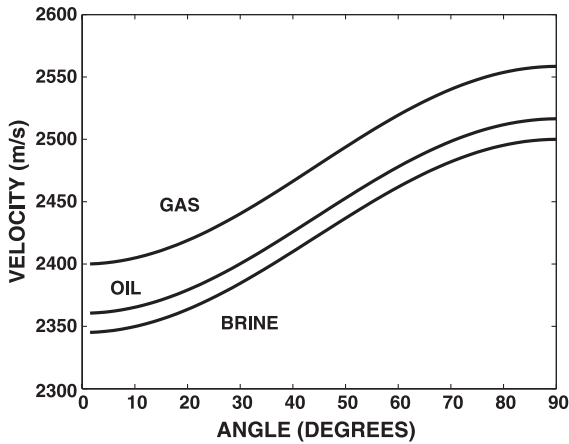


Fig. 11. Pure-shear velocity as a function of angle for three saturations. The frequency is 10 Hz and the fracture size is 1 m.

to the fracture normal, only density differences are important. The higher viscosity of the oil causes this velocity to be the highest at intermediate angles. Fig. 11 gives the analysis for the pure shear wave. In this case, only density differences are important.

Figs. 12 and 13 repeat the analysis with the frequency raised to 40 Hz. At this higher frequency, the viscosities of both the oil and the brine are important. Fig. 12 demonstrates that in this case the brine-saturated qP-velocity is now always comparable to the oil saturated qP-velocity. Fig. 13 shows that the brine-saturated quasi-shear velocity is closer to the oil-saturated velocity than was the case at 10 Hz, although

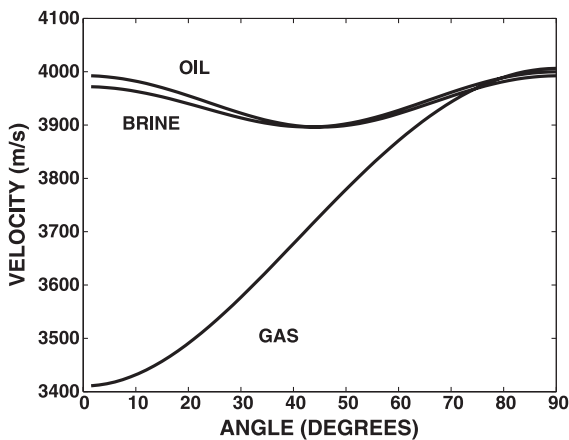


Fig. 12. qP velocity as a function of angle for three saturations. The frequency is 40 Hz and the fracture size is 1 m.

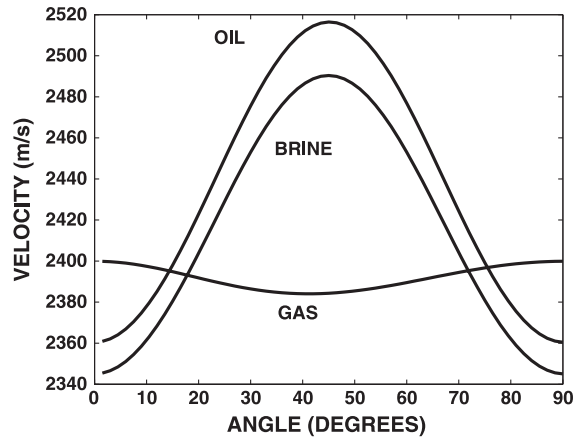


Fig. 13. Quasi-shear velocity as a function of angle for three saturations. The frequency is 40 Hz and the fracture size is 1 m.

the smaller density of the oil is still dominant. The behaviour of the pure shear wave is unchanged.

It is clear from the above discussion that we must expect the change in anisotropy between different saturations to depend on frequency. We conclude with an example to illustrate this effect. Assuming a fracture density of 0.1, we calculate percentage shear-wave splitting at an angle of propagation of 70° under brine and gas saturation for a range of fracture sizes and frequencies.

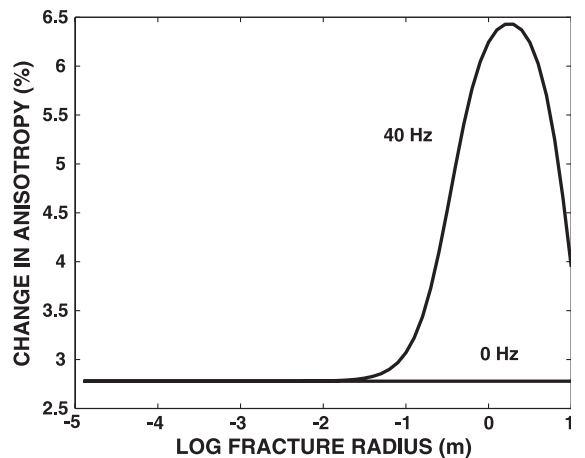


Fig. 14. Difference in percentage shear-wave splitting under brine and gas saturation as a function of the fracture radius for two different frequencies. Angle of propagation is 70° to the fracture normal, and fracture density is 0.1.

Fig. 14 shows the difference in anisotropy (percentage shear wave splitting under gas saturation minus percentage shear-wave splitting under brine saturation) as a function of the fracture radius for an assumed frequency of 40 Hz and the low-frequency limit of 0 Hz. For 40 Hz, there is a peak in the difference between the saturations for a fracture radius of 1m, while if we assume the low-frequency limit, there is no such peak. This highlights the dangers in assuming that seismic frequencies represent a low frequency, even when, as in this case, the squirt flow frequency as deduced from laboratory measurement lies above the sonic frequency band. The effect we demonstrate is consistent with the observations of Guest et al. (1998) concerning strong changes in shear wave splitting between brine and gas saturations.

## 6. Conclusions

We have given an alternative parameterisation for the model of Chapman (2003). Our method recognises the difficulties involved in predicting velocity from micro-structural information when porosity is high, and offers an alternative approach when “unfractured” velocities are known with reasonable precision. An advantage of the method is that it is not necessary to specify a “reference” elastic tensor, which cannot be measured.

The micro-structural isotropic crack density plays an important role in rock physics, but for certain applications, when the frequency is below the micro-structural squirt flow, the background velocities are known and matrix porosity is greater than fracture, it can be neglected. This is an important observation since it permits the elimination from the analysis of a further parameter, which can be difficult to estimate.

We test our approximations against the laboratory measurements on synthetic sandstone of Rathore et al. (1995). The only fitting parameter was the time scale constant  $\tau_m$ . Measured values were taken for all other parameters. A reasonable agreement is achieved, suggesting the validity of our approximations.

In the model, the elastic constants depend on frequency only through a non-dimensional parameter proportional to the product of frequency and

viscosity. Changing fluid viscosity therefore has a similar effect to changing the frequency of the wave. We argue that fluid viscosity effects should be taken into account when performing fluid substitution in anisotropic media. The change in shear-wave splitting between brine and gas saturation at seismic frequencies can be very much larger than is predicted by theories, which assume the low-frequency limit.

## Acknowledgements

This work is supported by the Natural Environment Research Council through contract GST22305 as part of the thematic programme Understanding the micro to Macro Behaviour of Rock Fluid systems, and by the sponsors of the Edinburgh Anisotropy Project (EAP). It is presented with the approval of the Executive Director of the British Geological Survey (NERC) and the EAP sponsors: Agip, BP, Chevron, Conoco, ExxonMobil, Landmark, Norsk Hydro, PGS, Phillips, Schlumberger, Shell, Texaco, Trade Partners UK and Veritas DGC.

## Appendix A

This appendix summarises the formulae given for the frequency-dependent, transversely isotropic elastic tensor given by Chapman (2003). The pore space in the rock was considered to consist of three components, a porosity associated with spherical pores,  $\Phi_p$ , an isotropic collection of microcracks with density  $\epsilon_c$  and a set of aligned spheroidal penny-shaped fractures with density  $\epsilon_f$  and radius (length of the major axis)  $a_f$ . The crack density is defined, following Hudson (1981) as  $Na^3/V$ , where  $N$  is the number of cracks in a volume  $V$  and  $a$  is the crack radius. The radii of the microcracks and pores are identified with the grain size  $\varsigma$ .

Two-time scale constants emerge from the analysis,  $\tau_m$  and  $\tau_f$ . The first constant  $\tau_m$  is the standard micro-structural squirt flow frequency. It was demonstrated by Chapman (2003) that:

$$\tau_f = \left( \frac{a_f}{\varsigma} \right) \tau_m. \quad (\text{A.1})$$

Chapman (2003) further defined:

$$\gamma = \frac{3\pi}{8(1-\nu)} \left( 1 + \frac{4}{3} \frac{\rho_s}{\rho_f} \left( \frac{V_s}{V_f} \right)^2 \right); \quad (\text{A.2})$$

where  $V_s$  is a representative shear velocity,  $V_f$  is the acoustic velocity in the fluid,  $\rho_f$  and  $\rho_s$  are the densities of the fluid and saturated rock, respectively, and  $\nu$  is the Poisson's ratio. When the method presented in the text of this paper is used,  $V_s$  should be identified with  $V_s^0$  and the Poisson's ratio calculated from  $\lambda^0$  and  $\mu^0$ . If  $\kappa_f$  denotes the fluid bulk modulus, we define:

$$K_c = \frac{\pi\mu^r}{2\kappa_f(1-\nu)}; \quad (\text{A.3})$$

$$K_p = \frac{4\mu}{3\kappa_f}; \quad (\text{A.4})$$

$$\gamma' = \gamma \frac{1-\nu}{1+\nu} \frac{1}{1+K_p}. \quad (\text{A.5})$$

For sufficiently small aspect ratios, we can take  $K_c = 0$ . We introduce the further notation:

$$l = \frac{4}{3} \frac{\pi\epsilon_c}{\pi\epsilon_c + \phi_p}; \quad (\text{A.6})$$

$$\beta = \frac{4}{3} \frac{\pi\epsilon_f}{\pi\epsilon_c + \phi_p}. \quad (\text{A.7})$$

Introducing  $\omega$  for the angular frequency, the frequency dependence is expressed through the functions:

$$D_1 = \left[ (1-l)\gamma + \frac{(1-l)\beta}{1+i\omega\tau_f} + \left( l + \frac{l\beta}{1+i\omega\tau_f} \right) \times \left( \frac{1+i\omega\gamma\tau_m}{1+i\omega\tau_m} \right) \right]^{-1} \times \left[ \frac{l}{3(1+K_c)} + (1-l)\gamma' - \frac{i\omega\tau_m}{1+i\omega\tau_m} \left( \frac{1}{3(1+K_c)} - \gamma' \right) \times \left( l + \frac{l\beta}{1+i\omega\tau_f} \right) \right]; \quad (\text{A.8})$$

$$D_2 = \left[ (1-l)\gamma + \frac{(1-l)\beta}{1+i\omega\tau_f} + \left( l + \frac{l\beta}{1+i\omega\tau_f} \right) \times \left( \frac{1+i\omega\gamma\tau_m}{1+i\omega\tau_m} \right) \right]^{-1} \times \left( \frac{\beta}{(1+K_c)(1+i\omega\tau_f)} \right); \quad (\text{A.9})$$

$$G_1 = \frac{i\omega\tau_m}{(1+K_c)(1+i\omega\tau_m)}; \quad (\text{A.10})$$

$$G_2 = \frac{1+i\omega\gamma\tau_m}{1+i\omega\tau_m} D_1 - \frac{i\omega\tau_m\gamma'}{1+i\omega\tau_m}; \quad (\text{A.11})$$

$$G_3 = \frac{1+i\omega\gamma\tau_m}{1+i\omega\tau_m} D_2; \quad (\text{A.12})$$

$$F_1 = \frac{1}{1+i\omega\tau_f} \left[ \frac{1+i\omega\gamma\tau_m}{1+i\omega\tau_m} l D_1 + (1-l) D_1 + \frac{i\omega\tau_m}{1+i\omega\tau_m} \left( \frac{1}{3(1+K_c)} - \gamma' \right) \right]; \quad (\text{A.13})$$

$$F_2 = \frac{1}{1+i\omega\tau_f} \times \left[ \frac{i\omega\tau_f}{1+K_c} + l \frac{1+i\omega\gamma\tau_m}{1+i\omega\tau_m} D_2 + (1-l) D_2 \right]. \quad (\text{A.14})$$

With the final notations ( $\lambda$  and  $\mu$  being reference elastic moduli,  $\kappa$  the reference bulk modulus):

$$L_2 = \lambda^2 + \frac{4}{3} \lambda \mu + \frac{4}{5} \mu^2; \quad (\text{A.15})$$

$$L_4 = \lambda^2 + \frac{4}{3} \lambda \mu + \frac{4}{5} \mu^2; \quad (\text{A.16})$$

we can give expressions for the frequency dependent elastic tensor. Taking the  $x_3$  direction as the axis of symmetry (corresponding to the direction of the

fracture normals), the five independent elastic constants are:

$$\begin{aligned}
 C_{1111} = & (\lambda + 2\mu) - \epsilon_c \left[ \frac{8L_2(1-\nu)}{3\mu} + \frac{128}{45} \frac{1-\nu}{(2-\nu)} \mu \right. \\
 & - \frac{8L_2(1-\nu)}{\mu} G_1 - \frac{8\kappa^2(1-\nu)}{\mu} G_2 \\
 & \left. - \frac{8\lambda\kappa(1-\nu)}{3\mu} G_3 \right] - \phi_p \left[ \frac{3}{4\mu} \frac{1-\nu}{1+\nu} \right. \\
 & \times \left( 3\lambda^2 + 4\lambda\mu + \frac{36+20\nu}{7-5\nu} \mu^2 \right) \\
 & - \left( 1 + \frac{3\kappa}{4\mu} \right) (3\kappa D_1 + \lambda D_2) \left. \right] \\
 & - \epsilon_f \left[ \frac{8\lambda^2(1-\nu)}{3\mu} - \frac{8\lambda\kappa(1-\nu)}{\mu} F_1 \right. \\
 & \left. - \frac{8\lambda^2(1-\nu)}{3\mu} F_2 \right]; \tag{A.17}
 \end{aligned}$$

$$\begin{aligned}
 C_{3333} = & (\lambda + 2\mu) - \epsilon_c \left[ \frac{8L_2(1-\nu)}{3\mu} + \frac{128}{45} \frac{1-\nu}{(2-\nu)} \mu \right. \\
 & - \frac{8L_2(1-\nu)}{\mu} G_1 - \frac{8\kappa^2(1-\nu)}{\mu} G_2 \\
 & \left. - \frac{8(\lambda+2\mu)\kappa(1-\nu)}{3\mu} G_3 \right] - \phi_p \left[ \frac{3}{4\mu} \frac{1-\nu}{1+\nu} \right. \\
 & \times \left( 3\lambda^2 + 4\lambda\mu + \frac{36+20\nu}{7-5\nu} \mu^2 \right) \\
 & - \left( 1 + \frac{3\kappa}{4\mu} \right) (3\kappa D_1 + (\lambda+2\mu)D_2) \left. \right] \\
 & - \epsilon_f \left[ \frac{8(\lambda+2\mu)^2(1-\nu)}{3\mu} \right. \\
 & - \frac{8(\lambda+2\mu)\kappa(1-\nu)}{\mu} F_1 \\
 & \left. - \frac{8(\lambda+2\mu)^2(1-\nu)}{3\mu} F_2 \right]; \tag{A.18}
 \end{aligned}$$

$$\begin{aligned}
 C_{2323} = & \mu - \epsilon_c \left[ \frac{32}{45} \mu(1-\nu)(1-G_1) + \frac{32}{45} \frac{1-\nu}{2-\nu} \mu \right] \\
 & - 15\phi_p \frac{1-\nu}{7-5\nu} \mu - \epsilon_f \frac{16(1-\nu)}{3(2-\nu)} \mu; \tag{A.19}
 \end{aligned}$$

$$\begin{aligned}
 C_{1122} = & \lambda - \epsilon_c \left[ \frac{8L_4(1-\nu)}{\mu} - \frac{64}{45} \frac{1-\nu}{(2-\nu)} \mu \right. \\
 & - \frac{8L_4(1-\nu)}{3\mu} G_1 - \frac{8\kappa^2(1-\nu)}{\mu} G_2 \\
 & \left. - \frac{8\lambda\kappa(1-\nu)}{3\mu} G_3 \right] - \phi_p \left[ \frac{3}{4\mu} \frac{1-\nu}{1+\nu} \right. \\
 & \times \left( 3\lambda^2 + 4\lambda\mu - \frac{4(1+5\nu)}{7-5\nu} \mu^2 \right) \\
 & - \left( 1 + \frac{3\kappa}{4\mu} \right) (3\kappa D_1 + \lambda D_2) \left. \right] \\
 & - \epsilon_f \left[ \frac{8\lambda^2(1-\nu)}{3\mu} - \frac{8\lambda\kappa(1-\nu)}{\mu} F_1 \right. \\
 & \left. - \frac{8\lambda^2(1-\nu)}{3\mu} F_2 \right]; \tag{A.20}
 \end{aligned}$$

$$\begin{aligned}
 C_{1133} = & \lambda - \epsilon_c \left[ \frac{8L_4(1-\nu)}{\mu} - \frac{64}{45} \frac{1-\nu}{(2-\nu)} \mu \right. \\
 & - \frac{8L_4(1-\nu)}{3\mu} G_1 - \frac{8\kappa^2(1-\nu)}{\mu} G_2 \\
 & \left. - \frac{8(\lambda+\mu)\kappa(1-\nu)}{3\mu} G_3 \right] - \phi_p \left[ \frac{3}{4\mu} \frac{1-\nu}{1+\nu} \right. \\
 & \times \left( 3\lambda^2 + 4\lambda\mu + \frac{4(1+5\nu)}{7-5\nu} \mu^2 \right) \\
 & - \left( 1 + \frac{3\kappa}{4\mu} \right) (3\kappa D_1 + (\lambda+\mu)D_2) \left. \right] \\
 & - \epsilon_f \left[ \frac{8\lambda(\lambda+\mu)(1-\nu)}{3\mu} \right. \\
 & - \frac{8(\lambda+\mu)\kappa(1-\nu)}{\mu} F_1 \\
 & \left. - \frac{8\lambda(\lambda+\mu)(1-\nu)}{3\mu} F_2 \right]. \tag{A.21}
 \end{aligned}$$

The symbol  $\Phi_{c,p}$  used in the main body of the text refers to the corrections to the elastic tensor proportional to  $\epsilon_c$  and  $\Phi_p$ .

## References

Brown, R., Korrington, J., 1975. On the dependence of the elastic properties of a porous rock on the compressibility of the pore fluid. *Geophysics* 40, 608–616.

- Chapman, M., 2001. Modelling the wide-band laboratory response of rock samples to fluid and pressure changes, PhD Thesis, University of Edinburgh.
- Chapman, M., 2003. Frequency-dependent anisotropy due to meso-scale fractures in the presence of equant porosity. *Geophys. Prospect.* 51, 369–379.
- Chapman, M., Zatsepin, S.V., Crampin, S., 2002. Derivation of a microstructural poroelastic model. *Geophys. J. Int.* 151, 427–451.
- Christensen, R.M., 1980. *Mechanics of Composite Materials* Wiley.
- Eshelby, J.D., 1957. The determination of the elastic field of an ellipsoidal inclusion, and related problems. *Proc. R. Soc. Lond., A* 241, 376–396.
- Gassmann, F., 1951. Über die Elastizität poroser Medien. *Vier. der Natur.*, vol. 96. Gesellschaft, Zurich, pp. 1–23.
- Guest, W.S., van der Kolk, C.M., Potters, J.H.H.M., 1998. The effect of fracture filling fluids on shear propagation. 68th Int. Ann. Mtg., SEG, Expanded Abstracts, 948–951.
- Hudson, J.A., 1980. Overall properties of a cracked solid. *Math. Proc. Camb. Philos. Soc.* 88, 371–384.
- Hudson, J.A., 1981. Wave speeds and attenuation of elastic waves in material containing. *Geophys. J. R. Astron. Soc.* 64, 133–150.
- Hudson, J.A., Liu, E., Crampin, S., 1996. The mechanical properties of materials with interconnected cracks and pores. *Geophys. J. Int.* 124, 105–112.
- Hudson, J.A., Pointer, T., Liu, E., 2001. Effective medium theories for fluid-saturated with aligned cracks. *Geophys. Prospect.* 49, 509–522.
- Mavko, G., Mukerji, T., Dvorkin, J., 1998. *The Rock Physics Handbook*. Cambridge Univ. Press, Cambridge, UK.
- Murphy, W.F., 1985. Sonic and ultrasonic velocities: theory versus experiment. *Geophys. Res. Lett.* 12, 85–88.
- Nur, A., 1971. Effects of stress on velocity anisotropy in rocks with cracks. *J. Geophys. Res.* 8, 2022–2034.
- Rathore, J.S., Fjaer, E., Holt, R.M., Renlie, L., 1995. P- and S-wave anisotropy of a synthetic sandstone with controlled crack geometry. *Geophys. Prospect.* 43, 711–728.
- Thomsen, L., 1995. Elastic anisotropy due to aligned cracks in porous rock. *Geophys. Prospect.* 43, 805–829.
- Tod, S.R., 2001. The effects on seismic waves of interconnected nearly aligned cracks. *Geophys. J. Int.* 146, 249–263.
- van der Kolk, C.M., Guest, W.S., Potters, J.H.H.M., 2001. The 3D shear experiment over the Natih field in Oman: the effect of fracture-filling fluids on propagation. *Geophys. Prospect.* 49, 179–197.
- Zimmerman, R.W., 1991. *Compressibility of Sandstones*. Elsevier Science Publishers, Amsterdam, The Netherlands.